

AN EFFICIENT LAYER CONSTRUCTION METHOD TO GENERATE ACCURATE PRINTING TOOLPATHS OF PERIODIC CELLULAR STRUCTURES FOR SELECTIVE LASER MELTING PROCESS

S. J. Tan*, X. Zhang*, L. P. Ding*, ¹Y. C. Zhang†

* College of Mechanical and Electrical Engineering, Nanjing University of Aeronautics
and Astronautics, Nanjing, 210016, P. R. China

† ICB-COMM, UMR 6303, CNRS, Univ. Bourgogne Franche-Comté, UTBM, Belfort,
France

Abstract

Limited by stereolithography file format, current data processing in additive manufacturing (AM) processing chain is time-consuming and has a loss of model precision in data transformation. However, both the CAD software and AM machine accept the input of more convenient and high-precision mathematical curve expressions. A predefined curved scanning pattern can be achieved in a galvanometer scanning system of selective laser melting (SLM) process, which can improve the scanning accuracy and efficiency for the shapes that can be represented by mathematical functions, e.g., circle. Therefore, this study proposes a layer construction-based method to directly generate the toolpaths for cellular structure with large file size. To demonstrate the proposed method, a case study on the toolpath generation for a flame arrestor element with a large quantity of curved fine channels, is presented. Compared with the conventional printing preparation methods, the proposed method reduces up to 90% of the total preparation time and achieves higher quality toolpaths.

Introduction

Benefiting from a layer-by-layer manufacturing way, AM process can deal with the problem of the fabrication of freeform geometry [1]. Nowadays, more and more multi-functional, and high-performance structures with extremely complex geometries are designed and manufactured via AM process [2~4]. However, when the issue comes to a massive fine porous structure, the shortcomings of the current AM process are showing. Firstly, limited by stereolithography (STL) file format, it is difficult for current data processing in AM chain to balance the accuracy of printing toolpaths and the efficiency of data transformation [5]. In general, the design software and the AM pre-processing software cannot handle such a large amount of data. However, the model itself can be described by some simple mathematical equations or other representations [6]. Secondly, as the design stage separating from the printing stage, it is hard to ensure whether the designed model can be manufactured with success or not at the first time [7]. Although design for AM (DfAM) is proposed to integrate AM constraints in the design processing [8~9], designers translate the AM processing information to three-dimensional (3D) geometric constrains [10~12], which has a big difference with the printing toolpaths. Due to this difference, it is inaccurate to evaluate the manufacturability of the designed model for AM processing only

¹ Corresponding author.

E-mail address: yicha.zhang@utbm.fr

through its geometry. Both the printing toolpaths and AM parameters are needed to analyze. In addition, the ability of the AM process is limited by the design and the AM pre-processing software. The generating algorithm of the toolpaths used in AM pre-processing has its limitations in dealing with small corner [13] and thin-wall region, especially in the porous structures.

Therefore, to meet the future demands for multi-functional and high-performance structures, especially structures with large quantity of fine pores, this paper proposed an efficient layer construction method to generate accurate printing toolpaths for the selective laser melting process, which integrates the design stage and the printing stage. The remainder of this paper is organized in the following: Section 2 presents the proposed method, Section 3 details the method with a case study of the design and fabrication of a flame arrester element, and Section 4 concludes this paper with perspectives on the future work.

Method

2.1. Method overview

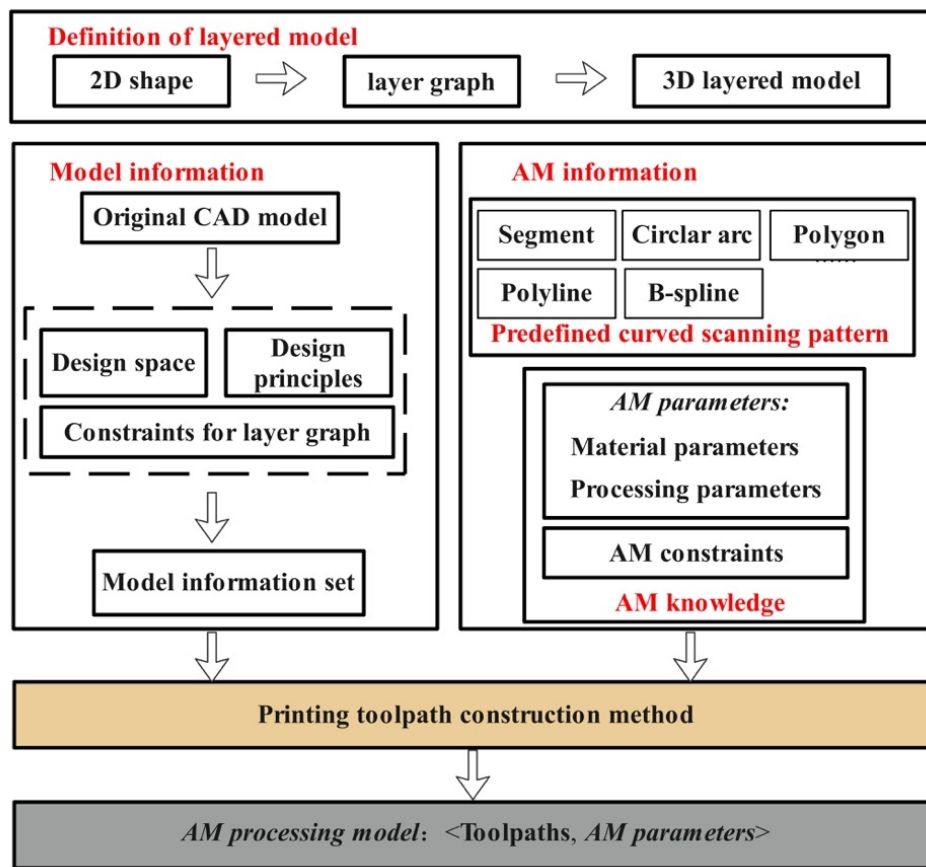


Figure 1. Framework of layer construction method integrated design and manufacturing.

The traditional data processing chain of AM includes model design, STL file creation, and build preparation[9]. It needs to transform the original CAD model to STL model, and the STL model to slicing model. For periodic cellular structure, this processing method usually causes the loss of printing accuracy and consumes a lot of time. Aiming to balance the accuracy and efficiency, the proposed method integrated design stage and AM printing stage, skipping the step

of model transformations. Figure 1 describes the framework of the proposed layer construction method, including four parts: a definition of layered model, information of the CAD model and AM process, a printing toolpath construction method, and an AM processing model. Here, we used this layered model instead of the traditional slicing model for toolpath generation. In the proposed method, a model information set that carries geometric constraints and design principles is reconstructed in the first step. Then, with the information of the original CAD model, the knowledge of AM (including AM parameters and AM constraints) and the predefined curved scanning patterns in the galvanometer scanning system, a printing toolpath construction method is used to generate the printing toolpaths. Finally, an AM processing model, including printing toolpaths and AM parameters is constructed and sent to the SLM printer. The detail of the proposed method is described in the following.

2.2. Definition of layered model

The mathematical definition of a 2D shape is given by the following equation (Eq. (1)), and Figure 2 describes an example of a 2D shape. In the conventional AM data processing chain, a polygon is used to approximate the curved shape, which loses the accuracy of boundary and increases the filling time of the toolpath. Here, we use curves directly and predefine these curves in the galvanometer scanning system.

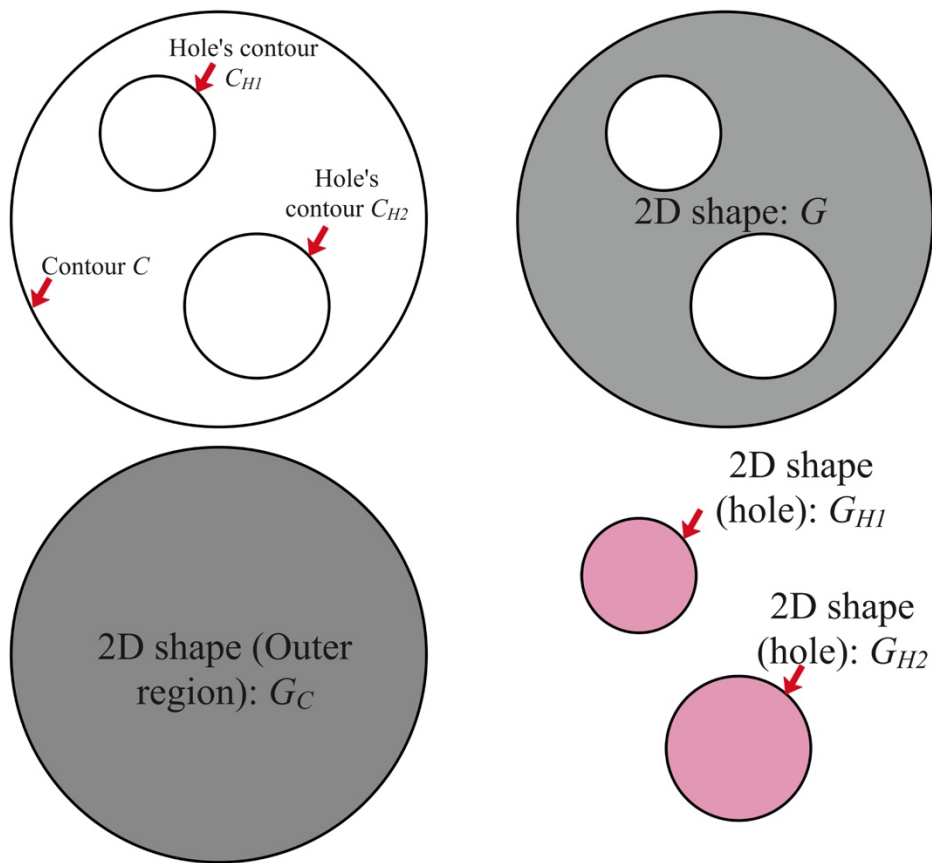


Figure 2. An example of 2D shape.

$$G = \Omega_C - \Omega_H = \Omega_C - (\Omega_{h_1} \cup \Omega_{h_2} \cup \dots \cup \Omega_{h_n}) \quad (1)$$

, where G is a 2D shape, Ω_c is the domain surrounded by contour C , and Ω_{h_i} is the i th domain surrounded by i th hole's contour C_{h_i} (not includes the boundary h_i). Ω_H is a domain which is united by Ω_{h_i} Ω_c , and Ω_{h_i} are given by Eqs. (2) and (3).

$$\Omega_c = \{(x, y) | f_c(x, y) \leq 0\} \quad (2)$$

$$\Omega_{h_i} = \{(x, y) | f_{h_i}(x, y) < 0\} \quad (3)$$

Here, as shown in Eq (4), we used the boundary representation method to storage the **2D shape**.

$$G = \langle C, H \rangle \quad (4)$$

$$C: f(x, y) = 0 \quad (5)$$

$$\text{For circle, } C_o: (x - x_o)^2 + (y - y_o)^2 - R^2 = 0 \quad (6)$$

$$H = \{C_{h_i} | i = 1, 2, 3, \dots, n\} \quad (7)$$

, where C is the contour (a closed curve, here is a circle) of the **2D shape**, C_{h_i} is the contour of the i th hole, H is a set of holes' contours, G is a 2D graph constituted by contour C and holes H , n is the number of holes in graph G .

Figure 3 presents an example of a 3D layered model, and Eq. (8) defines a 3D layered model. Unlike the conventional continuous representation of the 3D model, the 3D layered model is a discretized model, which can be used in the generation of AM toolpaths directly.

$$M = \{LG_i | i = 1, 2, 3, \dots, n\} \quad (8)$$

, where M is the 3D layered model, LG_i (as defined by Eq. (9)) is the layer graph model of the i th layer, n is the number of total layers of the model.

$$LG_i = \langle G_i, z_i \rangle \quad (9)$$

, where G_i is the **2D shape** in the i th layer, z_i is the height of the i th layer. For SLM process, z_i can be calculated as Eq. (10):

$$z_i = z_1 + (i - 1) * h \quad (10)$$

, where z_1 is the height of the first layer, and h is the layer thickness.

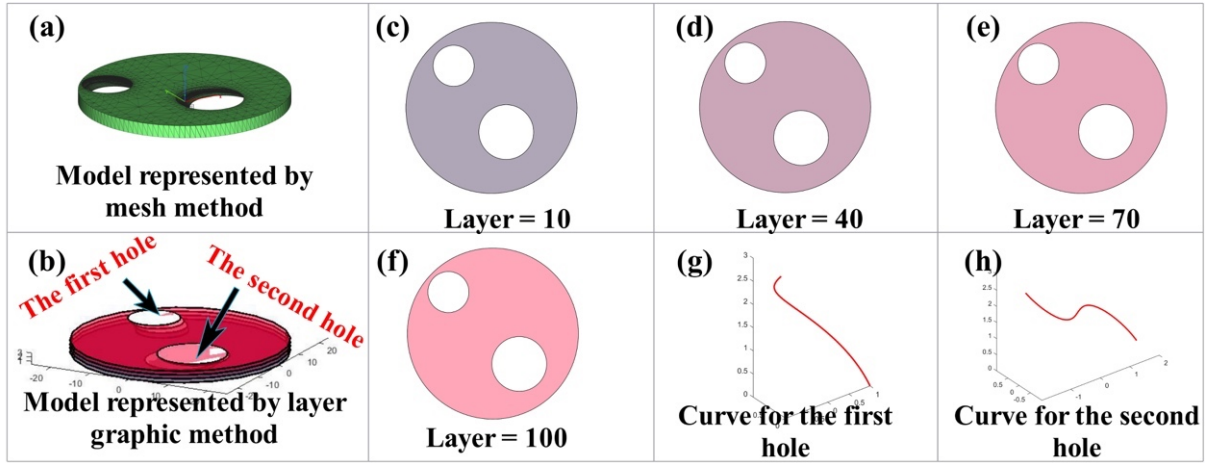


Figure 3. An example of a 3D layered model: (a) a STL format model. (b) a 3D layered model, 2D shapes of the (c) 10th layer, (d) 40th layer, (e) 70th layer, (f) 100th layer. (g) extruding curve for the first hole. (h) extruding curve for the second hole.

2.3. Model information set construction

As the STL format lacking the topological information of the model, it is unsuitable to use this format to represent the periodic cellular structure for slicing and toolpath **planning**. Referring to genes, they control the growth of animals and plants just by genetic information. Here, the model information set including the information of design space, constraints for layer graph and the design principles plays a role like a gene. However, there is no automatic method to **construct** the model information set because it needs human intelligence to extract the design principles according to the given model. For a sample model, slicing is an efficient way to obtain a layer graph, however, for the periodic cellular structure with complex shape, slicing is time-consuming. Hence, the hull model is used in this paper to construct the geometric constraints of the layer graph instead of the original model. Figure 4 shows an example of the reconstruction of the geometric constraints and design principles.

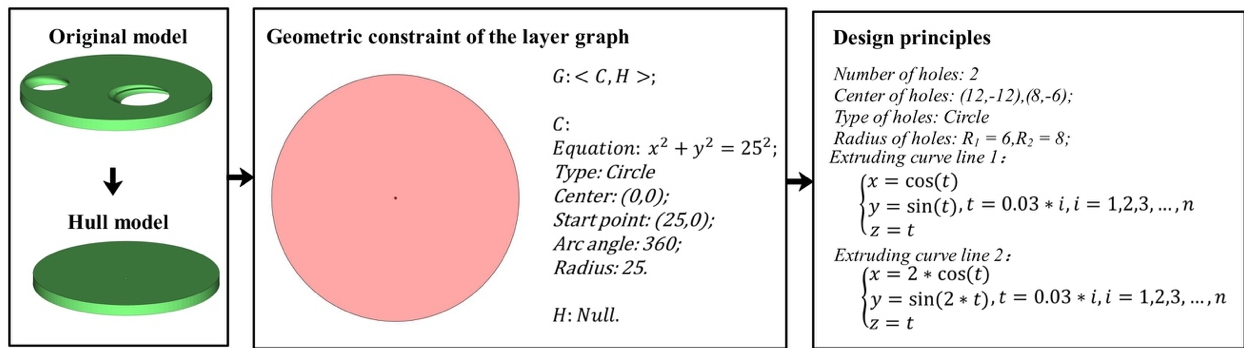


Figure 4. An example of the construction of the geometric constraints of layer graph and the design principles.

Hence, the model information set can be given by Eq. (11).

$$M_S = \langle \Omega_{2D}, DP \rangle \quad (11)$$

, where M_S is the model information set, Ω_{2D} is a set of geometric constraints for layer, and DP is the design principles.

2.4. AM information

2.4.1. Predefined scanning pattern in galvanometer scanning system

Except for the scanning patterns of line segment and polygon, the galvanometer offers a circular arc scanning pattern. Moreover, ellipse, B-spline and other curved scanning pattern are also available by predefining them in the controlling system of the galvanometer. Figure 5 presents the predefined circular arc scanning pattern in the galvanometer and the outputting format for the circular arc printing toolpath. Figure 6 presents the toolpaths and the corresponding scanning results using the predefined scanning patterns.

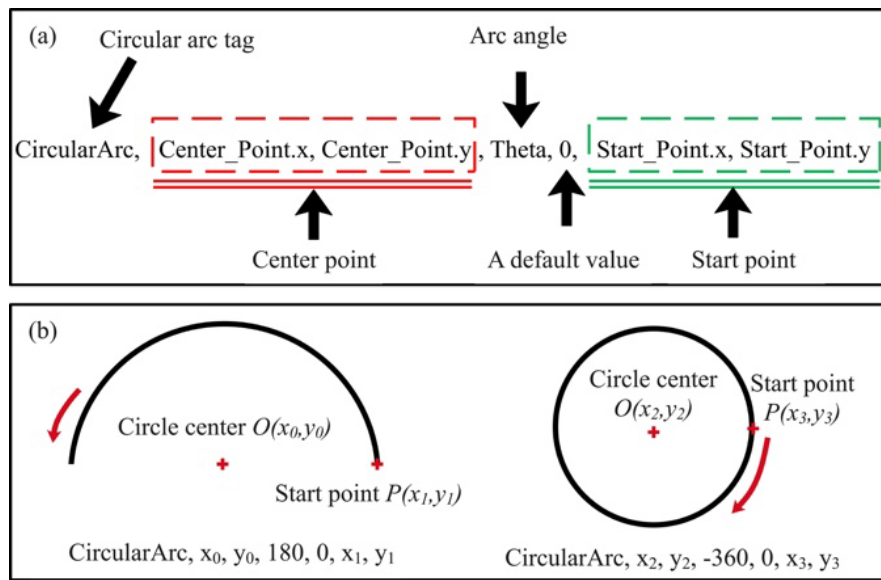


Figure 5. (a) outputting format for circular arc printing toolpath; (b) schematic diagram of the predefined circular arc scanning pattern in the galvanometer.

2.4.2. AM knowledge

In the proposed method, AM knowledge includes AM parameters and AM constraints. It is mathematically defined as Eq. (12), more information of AM knowledge can be found in [14]. However, it is challenging to translate all the AM processing constraints to design principles or filters. This paper focuses on the layer construction method integrated the design and AM and does not discuss more the AM processing parameters and constraints.

$$AMK = \langle AMpa, AMc \rangle \quad (12)$$

, where AMK is the AM knowledge, $AMpa$ is a set of AM parameters; $AMpa = \{Mp: \text{a set of material parameters}, Pp: \text{a set of processing parameters}\}$, AMc is a set of AM constraints.

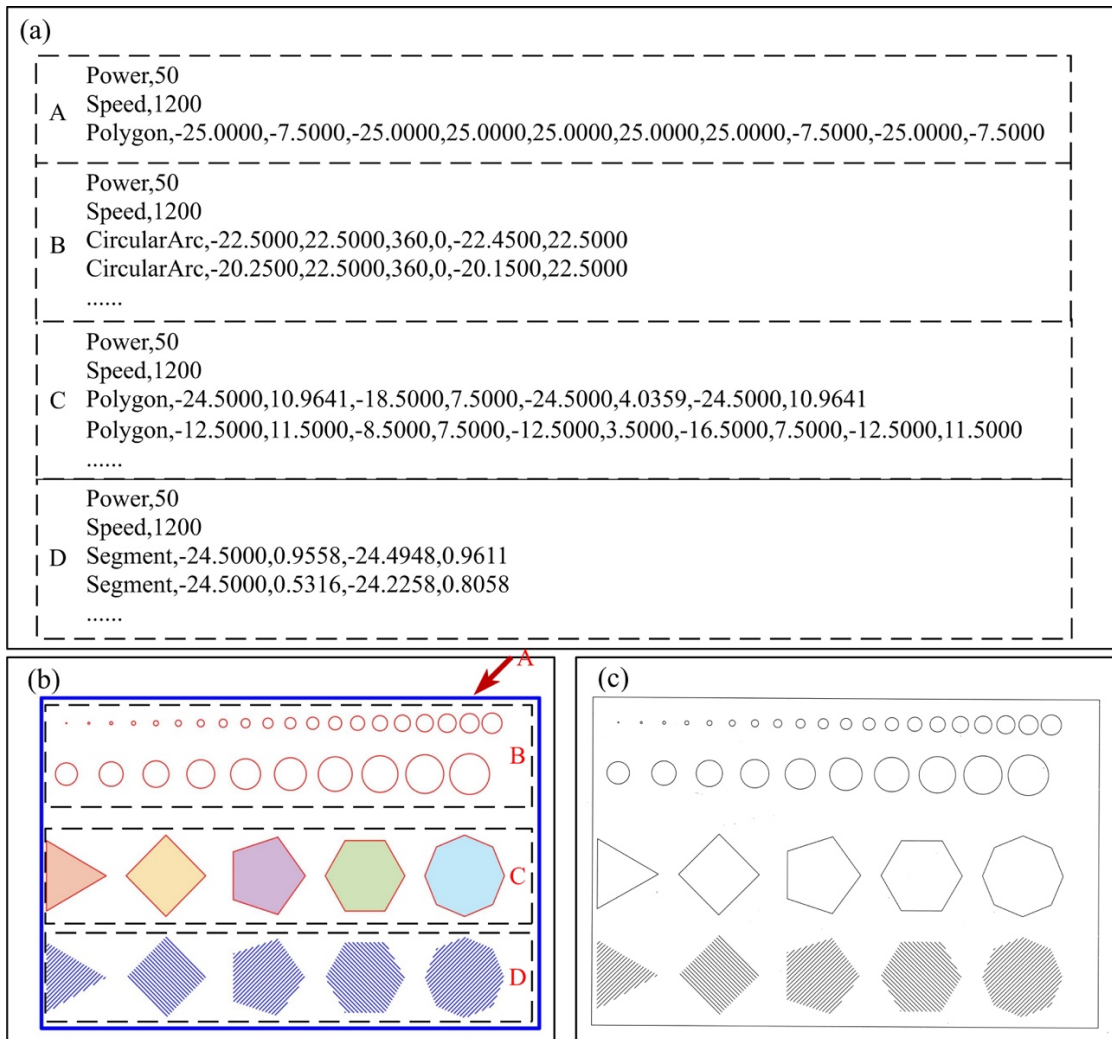


Figure 6. An example of printing toolpaths and the corresponding laser scanning results: (a) printing toolpaths; (b) the designed shapes; (c) the laser scanning results.

2.5. Printing toolpath construction method

As mentioned above, the conventional design & pre-processing method for AM process has limitations in balancing the accuracy and efficiency of the generation of printing toolpaths. Layer toolpath construction method [5] is a high-precision and high-efficiency toolpath generation method, connecting the design stage and printing stage for AM process. It divides the 3D design problem into many 2D design problems and generates toolpath directly. Figure 7 presents the workflow of the proposed printing toolpath construction method, and the main steps are described in the following:

Step 1. Construct 2D design space. 2D design space is needed in the proposed method. It offers the geometric constraints for the 2D graphic design. Designers obtain this 2D space by slicing the original 3D design space or even draw it directly for some simple shapes.

Step 2. Design 2D layer graph. Design principles, predefined scanning patterns and AM processing constraints are considered to design the 2D **shape**. Unlike conventional interactive design mode, we use parameterized method to design the 2D **shape** by MATLAB or Rhino

grasshopper. The type of the boundary is selected from the predefined scanning patterns in the galvanometer scanning system and a part of AM processing constraints are used in the size determinization, e.g., the cutting allowance. At this moment, only polygon, polyline, circle, circular arc, ellipse, and their combinations are allowed. Once the 2D layer graph is designed, another part of AM processing constraints, e.g., the overhang angle, are used as filters to check whether the 2D layer graph can meet the AM processing requirements.

Step 3. Generate layer toolpath. The toolpath is a set of predefined scanning patterns in galvanometer scanning system, attaching AM processing information, i.e., laser power, scanning speed. A homemade clipping algorithm is used to clip the segment pattern toolpath of the parallel segments that are inside of the 2D shape.

Step 4. Optimize layer toolpath. To reduce the printing time, the scanning directions of the segment patterns are set to 'Zigzag', and the scanning sequences of the different regions or contours are treated as a travel salesman problem (TSP), a genetic algorithm (GA) is used to solve this problem.

Step 5. Add toolpaths and parameters in AM processing model. The last step is to combine the toolpaths and other AM parameters, i.e., material parameters, AM processing parameters and add them in an AM processing model for outputting.

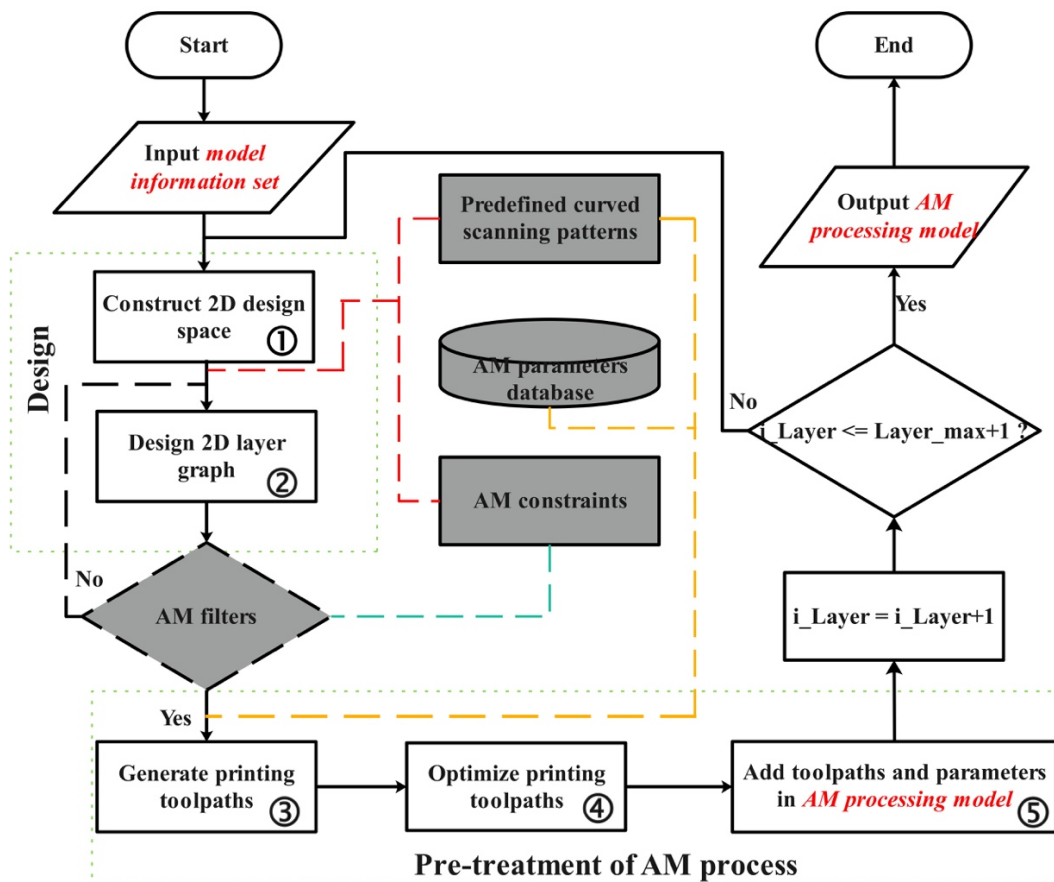


Figure 7. Workflow of the proposed printing toolpath construction method.

Case study

3.1. Original model

To demonstrate the method efficiency, a complex case, flame arrester, with periodic fine features from industry is selected. Figure 8 shows the original model of the flame arrester element. It has more than 10,000 holes and the STL model updating time is about 2 hours in a home computer (RAM: 4*8GB, *Crucial*, CPU: Xeon E5 2660 V4, *Intel*) with Rhino grasshopper.

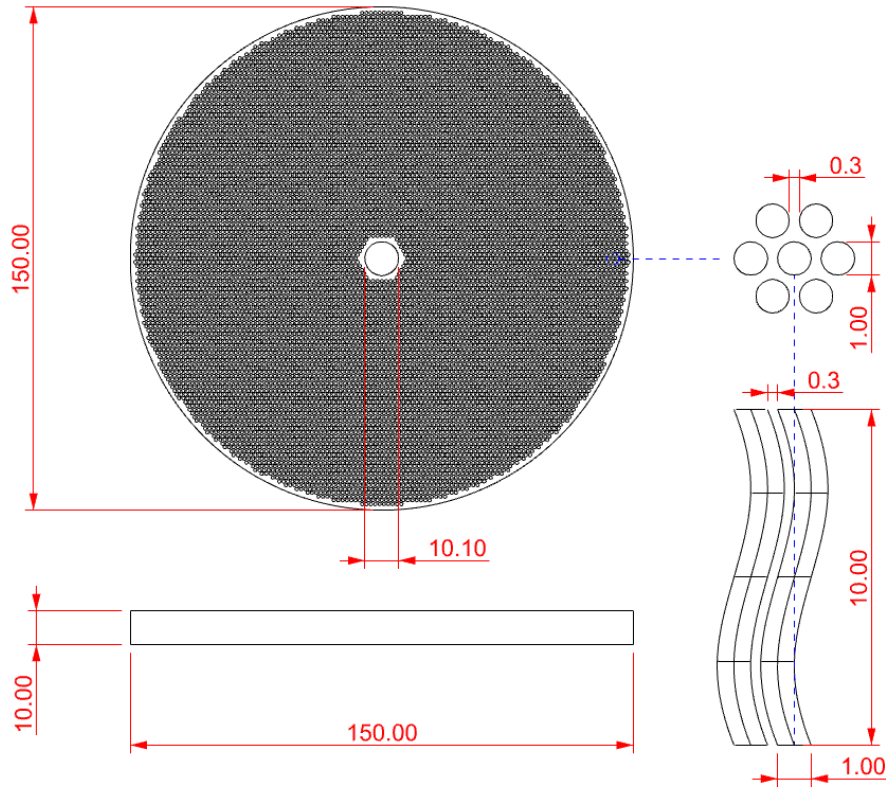


Figure 8. Original CAD model of the flame arrester element.

3.2. Layer graphic model reconstruction

3.2.1. Model information set of the flame arrester

According to Figure 3, many 2D shapes are designed to compose a 3D model instead of designing it directly. The 3D design space needs to be divided into 2D geometric constraints at a different height. The 2D geometric constraint of the flame arrester element at $z = z_i$ is given by Eq. (13).

$$\Omega_{R_1} = \Omega_c - \Omega_{h_0} = \{(x, y) | f_c(x, y) \leq 0\} - \{(x, y) | f_{h_0}(x, y) < 0\} = \{(x, y) | f_c(x, y) \leq 0, f_{h_0}(x, y) \geq 0\} \quad (13)$$

$$C: f_c(x, y) = x^2 + y^2 - 75^2 \quad (14)$$

$$h_0: f_{h_0}(x, y) = x^2 + y^2 - 5.05^2 \quad (15)$$

, where Ω_{R_1} is the 2D design domain for the graph in the first layer, Ω_c is a domain surrounded by contour C , Ω_{h_0} is a domain surrounded by hole's contour h_0 .

Except for the geometric constraints, the original model also exhibits the design principles, the results are given as follows:

(1) the circular holes are arranged at the vertices and the centers of hexagons in the hexagonal array; the hexagonal array at $z = z_1$ is defined by Eq. (16), the circles can be represented by Eq. (22), and the hole's region is given by Eq. (23).

$$S_{ce_1} = (S_{hp1} \cup S_{hp2}) \cap \Omega_f \quad (16)$$

$$S_{hp1} = \{(x, y) | x = x_0 + i * a, y = y_0 + j * \sqrt{3}a; i = 1, 2, 3, \dots m; j = 1, 2, 3, \dots n\} \quad (17)$$

$$S_{hp2} = \{(x, y) | x = x_0 - \frac{a}{2} + i * a, y = y_0 + \frac{\sqrt{3}a}{2} + j * \sqrt{3}a; i = 1, 2, 3, \dots m; j = 1, 2, 3, \dots n\} \quad (18)$$

$$\Omega_f = \Omega_{cof} - \Omega_{hof} = \{(x, y) | f_{cof}(x, y) \leq 0\} - \{(x, y) | f_{hof}(x, y) < 0\} \quad (19)$$

$$cof: f_{cof}(x, y) = x^2 + y^2 - 74^2 \quad (20)$$

$$hof: f_{hof}(x, y) = x^2 + y^2 - 6.05^2 \quad (21)$$

, where S_{ce_1} is a set of the centers of holes in the first layer, a is the side length of the hexagon, (x_0, y_0) is the start point of the hexagonal array, m and n are the point numbers in x and y direction, respectively, Ω_f is the filling domain, cof and hof are the two boundaries of Ω_f .

circles:

$$S_c = \{l_j | l_j(x, y): (x - x_j)^2 + (y - y_j)^2 = 1, (x_j, y_j) \in S_{ce_1}, j = 1, 2, 3, \dots k\} \quad (22)$$

hole's region:

$$\Omega_{H_1} = \{(x, y) | l_1(x, y) < 0\} \cup \{(x, y) | l_2(x, y) < 0\} \cup \dots \cup \{(x, y) | l_k(x, y) < 0\}; l_k \in S_{c_1} \quad (23)$$

, where S_c is a set of circles, l_j is the j th circle, k is the total point number in S_{ce_1} , Ω_{H_1} is the holes' region in the first layer.

(2) the circular holes are extruded along the curve, and the curve is defined by Eq. (24):

$$Ec: \begin{cases} x = \cos\left(\frac{\pi}{5} \times t\right) - 1; \\ y = \sin\left(\frac{\pi}{5} \times t\right); \\ z = t; \end{cases} \quad (24)$$

, where Ec is the extruding curve, (x, y, z) is the cartesian coordinate of a point, t is a parameter and $t \in [0, 10]$.

Hence, according to Eq. (11), the model information set of the flame arrester element can be represented as follows:

$$M_S = \langle \Omega_{2D}, DP \rangle = \langle \{\Omega_{R_1}, \Omega_{R_1}, \Omega_{R_1}, \dots, \Omega_{R_1}\}, \{Sc, Ec\} \rangle \quad (25)$$

3.2.2. Graphic construction of the flame arrester

According to the original model, the total height of the flame arrester element is 10mm. However, the printed sample will be cut from the substrate. It needs to design a cutting allowance for the flame arrester element. According to AM knowledge, the commonly used cutting allowance is 1mm and the layer thickness is 0.03mm. Hence, the 3D layered model of the flame arrester element can be achieved by Eq. (26):

$$M = \{ \langle G_i, z_i \rangle \mid i = 1, 2, 3, \dots, 366 \} \quad (26)$$

$$z_i = z_1 + (i - 1) * 0.03 \quad (27)$$

$$G_i = \Omega_{R_i} - \Omega_{H_i}; \Omega_{R_i} \in \Omega_{2D}; \Omega_{H_i} \in \Omega_{H2D} \quad (28)$$

, where M is the layered model of the flame arrester element, z_i is the i th layer height, and $z_1 = 0.03mm$, G_i is the i th layer graph, Ω_{2D} is given by Eq. (16), and Ω_{H2D} is given by Eq. (34) .

Figure 9 presents the first layer graph of the flame arrester element at the height of $z = 0.03mm$. As shown in Figure 9(a), the redesigned space for the flame arrester element is a cylinder with a hole. The geometric constraints for every layer keep the same, hence the geometric constraints of the flame arrester element can be given as follows:

$$\Omega_{2D} = \{ \Omega_{R_i} \mid i = 1, 2, 3, \dots, n \} = \{ \Omega_{R_1}, \Omega_{R_1}, \Omega_{R_1}, \dots, \Omega_{R_1} \} \quad (29)$$

, where Ω_{R_i} is the 2D design domain for the graph in the i th layer, and Ω_{2D} is a set of the 2D design domain Ω_{R_i} for the graph.

For the region of circular holes in different layer, according to the design principle (2), the centers of the holes in different layers can be calculated as Eq. (30):

$$S_{ce_i} = \begin{cases} S_{ce_1}; i = 1, 2, 3, \dots, 33 \\ \{ (x, y) \mid \begin{bmatrix} x \\ y \end{bmatrix} = \begin{bmatrix} x_S \\ y_S \end{bmatrix} + \begin{bmatrix} dx_i \\ dy_i \end{bmatrix}, (x_S, y_S) \in S_{ce_1}; i = 34, 35, 36 \dots 366 \end{cases} \quad (30)$$

, where S_{ce_i} is a set of centers of holes in the i th layer, (x_S, y_S) is a center in S_{ce_1} , dx_i and dy_i can be calculated by Eq. (31).

$$\begin{bmatrix} dx_i \\ dy_i \end{bmatrix} = \begin{bmatrix} \cos\left(\frac{\pi}{5} \times (i - 33) * 0.03\right) - 1 \\ \sin\left(\frac{\pi}{5} \times (i - 33) * 0.03\right) \end{bmatrix} \quad (31)$$

Hence, the holes' region in different layers can be calculated as Eq. (32), and the set of the holes' region in different layers is given by Eq. (34).

hole's region:

$$\Omega_{H_i} = \{(x, y) | l_1(x, y) < 0\} \cup \{(x, y) | l_2(x, y) < 0\} \cup \dots \cup \{(x, y) | l_k(x, y) < 0\}; \quad l_k \in S_{c_i} \quad (32)$$

$$S_{c_i} = \{l_j | l_j(x, y): (x - x_j)^2 + (y - y_j)^2 = 1, (x_j, y_j) \in S_{ce_i}, j = 1, 2, 3, \dots, k\} \quad (33)$$

$$\Omega_{H2D} = \{\Omega_{H_i} | i = 1, 2, 3, \dots, n\} \quad (34)$$

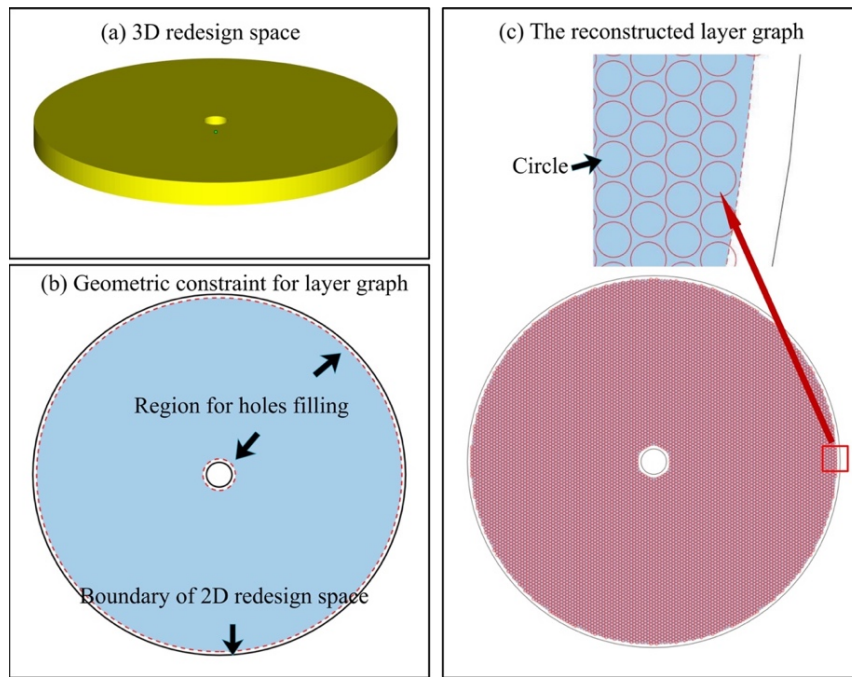


Figure 9. Layer graph of the flame arrester element.

A $\text{Ø}150\text{mm} * 10\text{mm}$ flame arrester element was manufactured for delivery under an argon protective atmosphere. Meanwhile, a $\text{Ø}50\text{mm} * 10\text{mm}$ sample with the same design principles was selected for comparison. The toolpaths were generated by MATLAB with a homemade filling algorithm. Moreover, for comparison, a STL model of the $\text{Ø}50\text{mm} * 10\text{mm}$ sample was designed by Rhino grasshopper and **sliced by Magics Build processor (BP) with the same parameters as the proposed method**. Except for the toolpaths' parameters, other AM parameters, e.g., material parameters, AM processing parameters are also required. Table 1 presents the processing parameters of the toolpaths, and Table 2 presents the other parameters used in the manufacturing.

Table 1. The processing parameters of the toolpaths

Name	Color	Type	Power(W)	Speed(mm/s)	Distance(mm)
Graphic boundary	black	Circular arc	-	-	-
Printing contour	red	Circular arc	120	650	0.065
Extra printing contour	blue	Circular arc	100	450	0.085
Filling line	red	Segment	135	850	0.085

Table2. The main parameters used in the manufacturing of the flame arrester element.

Name	Value
Layer thickness (mm)	0.03
Spot compensation (mm)	0.065
Extra contour number	1
Filling angle (°)	60
Angle increment (°)	67
Filling region offset distance (mm)	0
Material	Ti6Al4V
Protective gas	Ar
Oxygen content	< 100ppm
Gas flow (L/min)	3

After the generation of the printing toolpaths , the experiment was conducted using a commercial SLM printer (Ti150, *Profeta, Nanjing, China*). The Ti150 machine is equipped with an IPG photonics fiber laser (*German*) and a ScanLab galvanometer (*German*). The printing material is Ti6Al4V powder, supplied by ZhongHangMaiTe (*China*). Once the samples are printed, a stress relief annealing process is conducted and a wire electrical discharge machine is used to cut the sample from the substrate.

3.4. Results

Figure 10(a), (c) and (d) present the printing toolpaths of the first layer in the flame arrester elements. Figure 10(b) and (e) show the print samples. In the proposed method, all the filling toolpaths are selected from the predefined curved scanning patterns in the galvanometer. They are more accurate than the sliced contour of the STL model. Table 3 shows the comparison results of the time consumed by the layer construction method and traditional design & slicing method. The new method almost reduces 90% of the data processing time in AM processing chain.

Table 3. The comparison results of the time consumed by the layer construction method and traditional design & slicing method.

No	Size	Method	Model updating	Input and output	Toolpaths generation
1-1	Ø50mm *10mm	Layer construction	Null	Null	25 min (By MATLAB)
1-2	Ø50mm *10mm	Traditional design & slicing	30 min (By Rhino)	5 min	7 h (By Magics BP)
2-1	Ø150mm *10mm	Layer construction	Null	Null	2 h (By MATLAB)
2-2	Ø150mm *10mm	Traditional design & slicing	2h (By Rhino)	25 min	>2 days (By Magics BP)

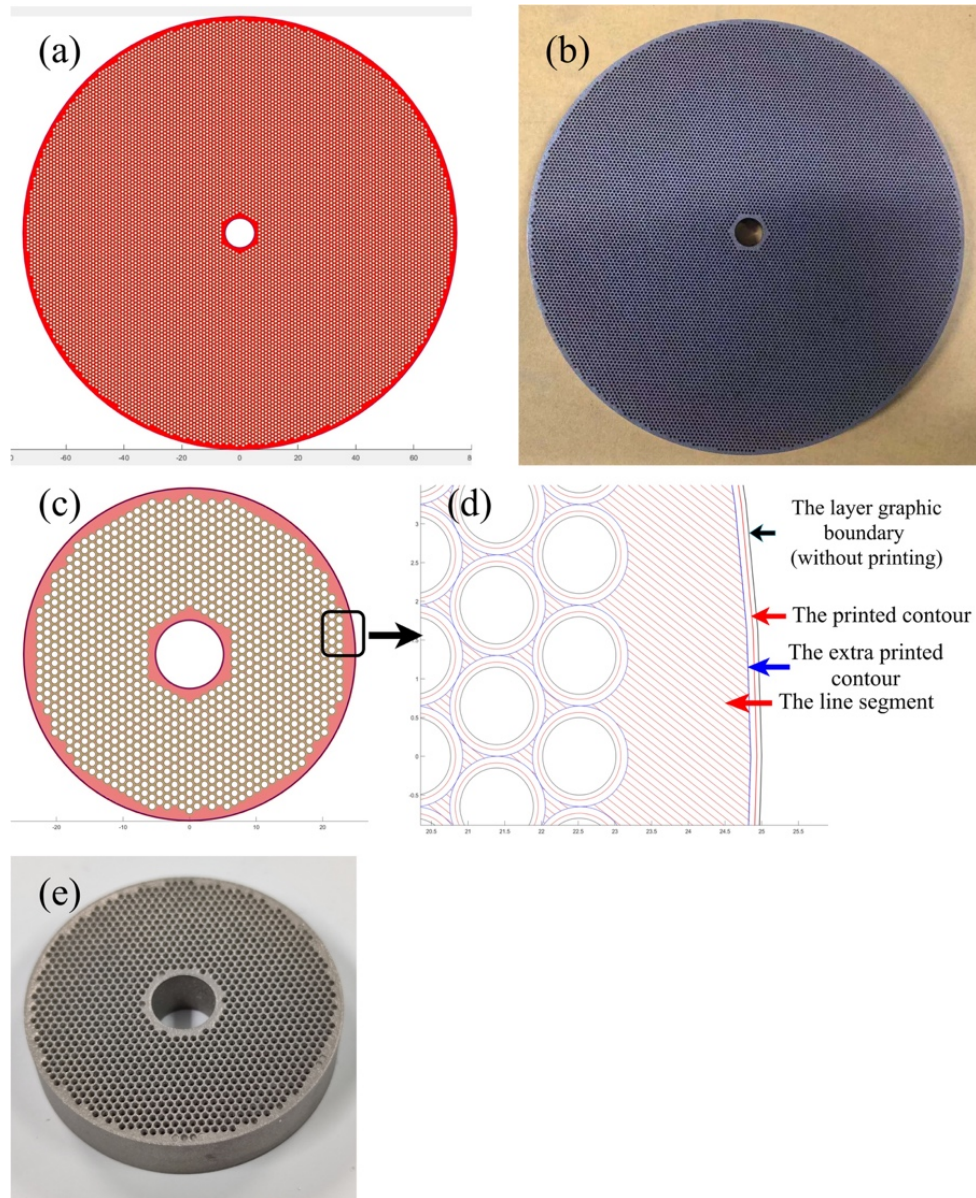


Figure 10. Printing toolpaths and results: (a) toolpaths of the first layer in the Ø150mm *10mm flame arrester element, (b) printing result of the Ø150mm *10mm flame arrester element, (c) toolpaths of the first layer in the Ø50mm *10mm flame arrester element, (d) a description of the toolpaths , (e) printing result of the Ø50mm *10mm flame arrester element.

Conclusions

The paper proposed a novel layer construction method of periodic cellular structure for AM process, integrating the design stage and printing stage. It is much more efficient than the traditional design & slicing method. It has potential application in the high performance and multifunctional structure with complex geometries. However, there is still a lot of work that needs to be done in the future to improve this method, e.g., spline scanning pattern and efficient filling algorithm. Meanwhile, in the proposed method, the model information set is constructed according to the original model. However, the original model is not necessary, designers can design the layer graph or toolpath directly rather than reconstructing it.

Reference:

- [1] Du Plessis, A., Broeckhoven, C., Yadroitsava, I., Yadroitsev, I., Hands, C. H., Kunju, R. and Bhate, D. (2019) "Beautiful and Functional: A Review of Biomimetic Design in Additive Manufacturing", *Additive Manufacturing*, Vol.27 No., pp: 408-427.
- [2] Kumar, V., Cormier, D. and Harrysson, O. (2012) "Electrical conductivity of hexagonal periodic lattice structures", *Virtual and Physical Prototyping*, Vol.7 No.1, pp: 81-90.
- [3] Kim, S. H., Yeon, S., Lee, J. H., Kim, Y. W., Lee, H., Park, J., Lee, N., Choi, J. P., Aranas, C., Lee, Y. J., An, S., Choi, K. and Son, Y. (2020) "Additive manufacturing of a shift block via laser powder bed fusion: the simultaneous utilisation of optimised topology and a lattice structure", *Virtual and physical prototyping*, Vol.15 No.4, pp: 460-480.
- [4] Pham, M., Liu, C., Todd, I. and Lertthanasarn, J. (2019) "Damage-tolerant architected materials inspired by crystal microstructure", *Nature*, Vol.565 No.7739, pp: 305-311.
- [5] Zhang, Y., Tan, S., Ding, L. and Bernard, A. (2021) "A toolpath-based layer construction method for designing & printing porous structure", *CIRP Annals*. <https://doi.org/10.1016/j.cirp.2021.04.020>.
- [6] Amado-Mendes, P., Godinho, L., Carbajo, J. and Ramis-Soriano, J. (2019) "Numerical modelling of finite periodic arrays of acoustic resonators using an efficient 3D BEM model", *Engineering Analysis with Boundary Elements*, Vol.102, pp: 73-86.
- [7] Paul, R. and Anand, S. (2015) "A combined energy and error optimization method for metal powder based additive manufacturing processes", *Rapid Prototyping Journal*, Vol.21 No.3, pp: 301-312.
- [8] Thompson, M. K., Moroni, G., Vaneker, T., Fadel, G., Campbell, R. I., Gibson, I., Bernard, A., Schulz, J., Graf, P., Ahuja, B. and Martina, F. (2016) "Design for Additive Manufacturing: Trends, opportunities, considerations, and constraints", *CIRP Annals*, Vol.65 No.2, pp: 737-760.
- [9] Vaneker, T., Bernard, A., Moroni, G., Gibson, I. and Zhang, Y. (2020) "Design for additive manufacturing: Framework and methodology", *CIRP Annals*, Vol.69 No.2, pp: 578-599.
- [10] Liu, J. and To, A. C. (2017) "Deposition path planning-integrated structural topology optimization for 3D additive manufacturing subject to self-support constraint", *Computer-Aided Design*, Vol.91, pp: 27-45.
- [11] Wang, C., Qian, X., Gerstler, W. D. and Shubrooks, J. (2019) "Boundary Slope Control in Topology Optimization for Additive Manufacturing: For Self- Support and Surface Roughness", *Journal of Manufacturing Science and Engineering-Transactions of the ASME*, Vol.141: 091001-1.
- [12] Wang, Z., Zhang, Y., Bernard, A. (2021) A constructive solid geometry-based generative design method for additive manufacturing. *Additive Manufacturing*. Vol. 41:101952.
- [13] Yu-an, J., Yong, H., Jianzhong, F., Wenfeng, G. and Zhiwei, L. (2014) "Optimization of tool-path generation for material extrusion-based additive manufacturing technology", *Additive manufacturing*, Vol.1-4, pp: 32-47.
- [14] Ko, H., Witherell, P., Lu, Y., Kim, S. and Rosen, D. W. (2020) "Machine learning and knowledge graph based design rule construction for additive manufacturing", *Additive Manufacturing*, Vol.37:101620.